Journal of Materials Chemistry C

Fluorination increases the electron mobility of zinc azadipyrromethene-based electron acceptors and enhances performance of fullerene-free organic solar cells

Journal:	*Journal of Materials Chemistry C*
Manuscript ID	TC-ART-12-2017-005820.R1
Article Type:	Paper
Date Submitted by the Author:	18-Feb-2018
Complete List of Authors:	Pejić, Sandra; Case Western Reserve Univ, Chemistry Thomsen, Anna; Case Western Reserve University, Chemistry Etheridge, Forrest; Case Western Reserve Univ, Chemistry Fernando, Roshan; Case Western Reserve University, Chemistry Wang, Chunlai; Case Western Reserve University, Chemistry Sauve, Genevieve; Case Western Reserve Univ, Chemistry

Journal of Materials Chemistry C

ARTICLE

Fluorination increases the electron mobility of zinc azadipyrromethene-based electron acceptors and enhances performance of fullerene-free organic solar cells

Received 00th January 20xx,
Accepted 00th January 20xx

DOI: 10.1039/x0xx00000x

www.rsc.org/

Sandra Pejić, Anna M. Thomsen, Forrest S. Etheridge, Roshan Fernando, Chunlai Wang, and Geneviève Sauvé*

Structure-property studies were performed on a series of four fluorinated zinc azadipyrromethene derivatives. The series is based on bis[2,8-diphenylethynyl-1,3,7,9-tetraphenylazadipyrromethene]zinc(II) ($Zn(WS3)_2$), with a fluorine atom either at the para position of the proximal phenyls, the distal phenyls or the pyrrolic phenylethynyls, refered to as the proximal, distal and pyrrolic positions, respectively. In order to study the degree of fluorination we also added $-CF_3$ to the pyrrolic positions. All compexes had similar absorption spectra, 600-800nm in films, complementing the absorption of the well-known donor poly(3-hexylthiophene) (P3HT). The chelates were tested in bulk heterojunction organic photovoltaic (OPV) devices using P3HT as the electron donor. Compared to the unfluorinated acceptor $Zn(WS3)_2$, fluorination increased power conversion efficiencies (PCEs) in all cases except in the proximal position. The best results were obtained when either F or CF_3 were added to the pyrrolic positions, with a PCE of 3.3% and 3.7%, respectively. Atomic force microscopy images revealed a favorable phase separation and showed no sign of large-scale aggregation for all blends. Light intensity measurements revealed that bimolecular recombination limits performance in these fullerene-free devices, and that the addition of fluorine suppressed bimolecular recombination, with the largest suppression seen with the pyrrolic substitutions F and CF_3. Electron mobility increased with fluorination, again with the largest increase when adding fluorines to the pyrrolic positions, reaching mobilities as high as ~10^{-3} $cm^2V^{-1}s^{-1}$, on par with electron mobility of the ubiquitous phenyl-C_{61}-butyric acid methyl ester (PCBM) acceptor in blends. These results point to the importance of the pyrrolic phenylethylnyls chemical composition for optimizing charge transport and device performance for these type of complexes.

Introduction

Fluorination is increasingly used to tune properties and improve device performance of organic semiconductors in organic photovoltaics (OPVs) (2-6). Fluorine atoms are effective electron withdrawing groups due to their strong electronegative properties and small size. Fluorination of conjugated systems is known to lower both the highest occupied molecular orbital (HOMO) and the lowest unoccupied molecular orbital (LUMO) levels, increase stability towards oxidative degradation, enable n-type or ambipolar semiconductivity, and enhance planarity and charge carrier mobility via intramolecular fluorine interactions (7-14). Since the maximum open-circuit voltage (V_{OC}) in OPVs is related to the energy difference between HOMO of the donor and LUMO of the acceptor, the addition of electron withdrawing groups to the donor has been shown to lower its HOMO energy level and increase V_{OC} (6, 15). Others have reported that fluorination can increase short-circuit current density (J_{SC}) and fill factor (FF) by suppressing bimolecular and geminate recombination (16-18). All of these factors indicate that adding fluorine is a valuable tool for increasing device performance.

*Department of Chemistry, Case Western Reserve University, Cleveland, OH 44106 USA. *E-mail : geneveive.sauve@case.edu*

Electronic Supplementary Information (ESI) available: [details of any supplementary information available should be included here]. See DOI: 10.1039/x0xx00000x

Fullerene derivatives are popular as acceptors in OPVs because they have good electron accepting properties, isotropic electron mobility, and form favorable nanoscale phase separation when blended with donors. However, they do not contribute significantly to light harvesting past 600 nm and have poor energy level tunability (19, 20). These shortcomings have motivated groups to study non-fullerene small molecules as electron acceptors and have recently reached PCEs as high as 14% (14, 21-26). We have explored azadipyrromethene (ADP) dyes and their Zn(II) complexes as non-fullerene electron acceptors due to their high electron affinity and intense absorption in the visible to the near-infrared region of the light spectra. The best device performance was obtained when a phenylethynyl moiety was installed in the pyrrolic positions, $Zn(WS3)_2$ (Figure 1) (27). $Zn(WS3)_2$ absorbs from 600-800 nm, which is complementary to the absorption spectra of P3HT, from 400-650 nm. In 2014, we reported a PCE of 4.1% when blended with poly(3-hexylthiophene) (P3HT) and atomic force microscopy (AFM) revealed a favorable nanoscale phase separation (28). However, the LUMO energy level of $Zn(WS3)_2$ is higher than that of PCBM, which limits the use of $Zn(WS3)_2$ as an electron acceptor.

In order to deepen the energy levels and increase its electron accepting properties, we added a single fluorine atom to three different positions on the parent compound, $Zn(WS3)_2$ at: the proximal phenyls (L1), the distal phenyls (L2) and on the

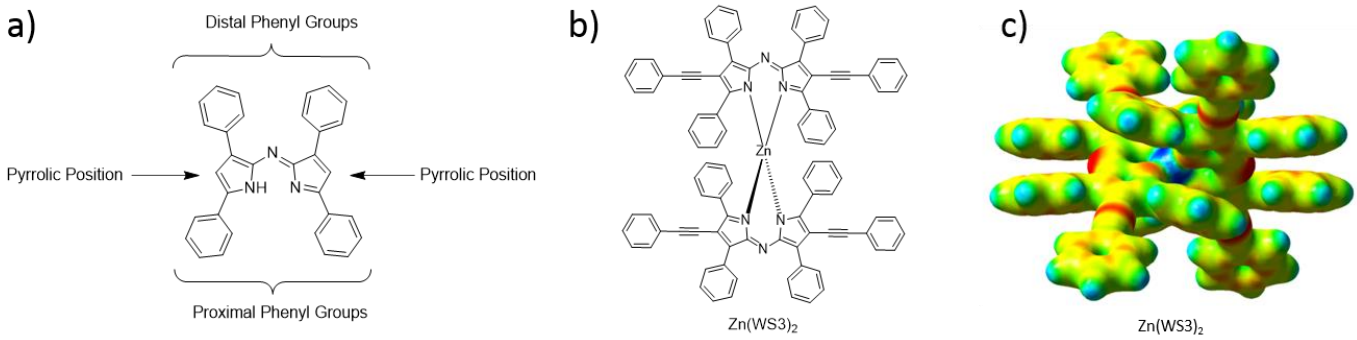

Fig. 1 Structures of non-fullerene azadipyrromethene-based acceptor; a) azadipyrromethene ligand labelling positioning b) chemical structure of $Zn(WS3)_2$ c) electrostatic potential surface of $Zn(WS3)_2$.

phenylethynyls in the pyrrolic position (L3) (1). A CF_3 group was also installed in the later position to study the degree of fluorination (L4). These ligands were chelated with Zn(II) and their structures are shown in Figure 2. We reported that neat film absorbance ~500-800 nm did not change drastically with the addition of fluorine, except for a small blue shift of ~19 nm (1). Cyclic-voltammetry measurements in solution revealed that the addition of fluorine did not have a large impact on the energy levels. The largest effect was observed for $Zn(L1)_2$ and $Zn(L4)_2$, with LUMO energy levels ~0.1 eV lower than that of $Zn(WS3)_2$ and approaching that of PCBM(1).

Here, we blended our acceptors with P3HT as the donor and tested their performance in OPVs. PCE increased with fluorination in all cases except in P3HT:$Zn(L1)_2$. Our current best PCE for the unfluorinated acceptor, $Zn(WS3)_2$, is 2.5%. Fluorination at the para position of the phenylethynyls gave the best performances, with a PCE of 3.74% for $Zn(L3)_2$ and 3.26% for $Zn(L4)_2$. The later also gave the highest J_{SC}, which combined with its lower LUMO energy level than $Zn(WS3)_2$, is promising for blending with other donors with lower-lying energy levels. To understand our results, we explored the effect of fluorination on bimolecular recombination and charge carrier mobility. Fluorination at the phenylethynyls proved to be highly beneficial in both reducing bimolecular recombination and enhancing electron mobility.

Experimental

UV-vis absorption was performed using a UV-Cary 50 spectrophotometer in o-DCB. For film absorption, glass

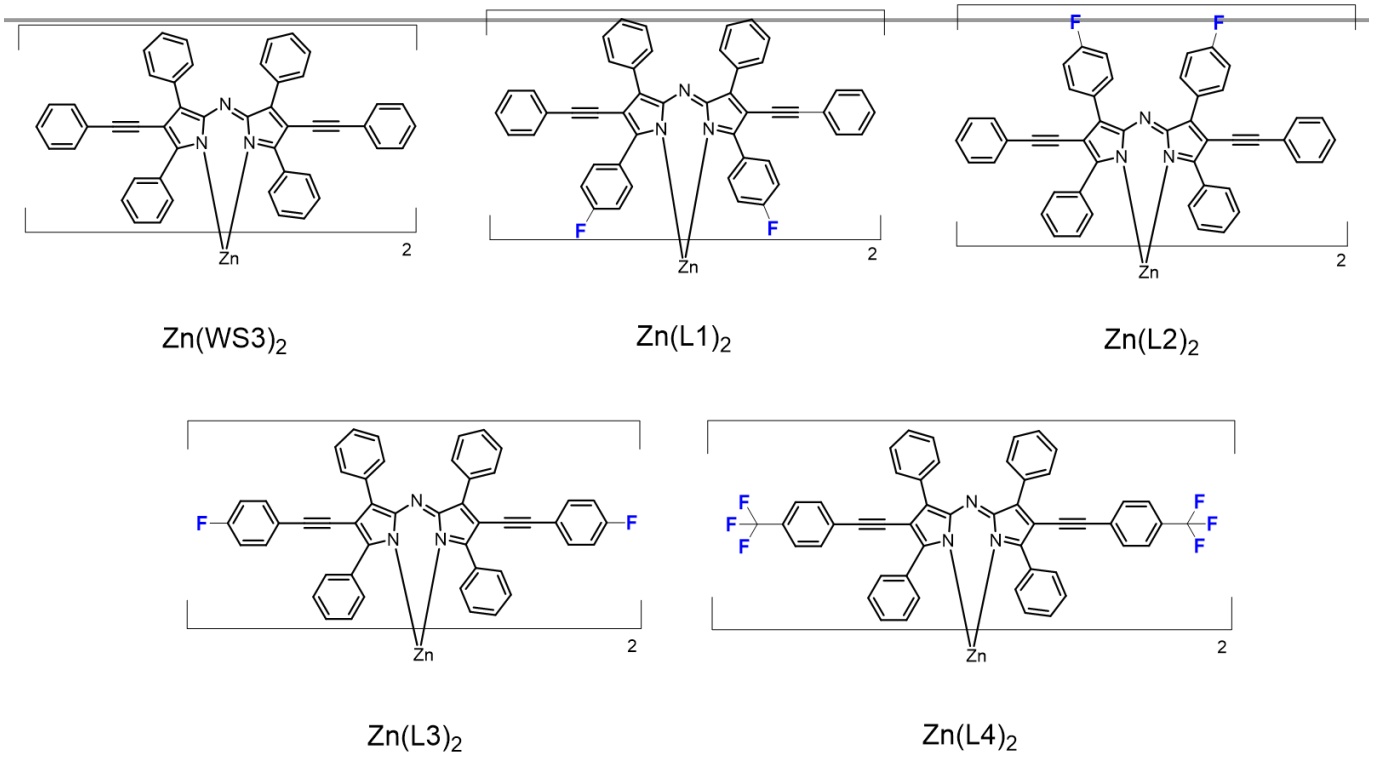

Fig. 2 Chemical structures of $Zn(WS3)_2$, $Zn(L1)_2$-$Zn(L4)_2$.

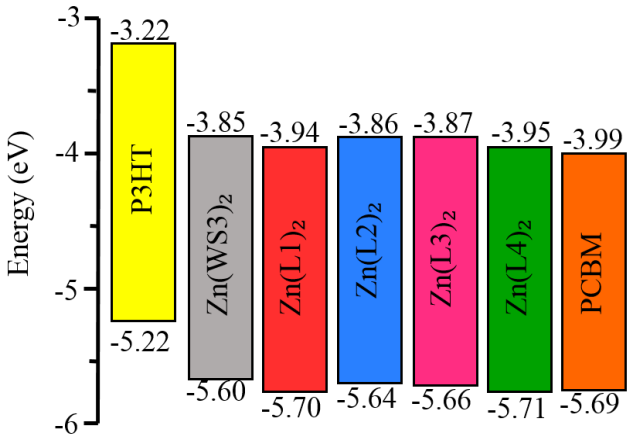

Fig. 3 Estimated HOMO/LUMO energy levels, using Fc/Fc^+ = -5.1 eV. Measurements for the Zn(II) complexes and PCBM were obtained in our laboratory in solution from the $E_{1/2}$ values, whereas that of P3HT was obtained in film from the oxidation onset and optical gap (1).

substrates were cleaned stepwise in soapy water, DI water, acetone and isopropanol under ultrasonication for 15 minutes. Solutions for film were prepared from a 10 mg/mL concentration and filtered through a 0.45µm PTFE filter. The films were spin coated at 400 rpm for 60 seconds. Blend films were prepared using the same optimized donor-to-acceptor ratio and concentrations as the active layer of photovoltaic devices. All films were annealed at 120°C for 30 minutes.

Photovoltaic properties were studied using the inverted configuration: ITO/ZnO/P3HT:Acceptor/MoO_3/Ag. ITO-coated glass substrates (R=15Ω/sq) were cleaned stepwise in soapy water, DI water, acetone and isopropanol under ultrasonication for 15 minutes followed by UV-ozone treatment at 80°C for 15 minutes. A ZnO layer was prepared from a precursor solution of 0.25M zinc acetate dihydrate in 0.25M ethanolamine and 2-methoxyethanol by spin coating at 4000 rpm for 40 seconds, then heated at 150°C for 7 minutes. The photoactive layers were spin coated inside the glovebox (PureLab^{HE}) at 1000 rpm for 40 seconds followed by 2000 rpm for 2 seconds from a blend solution with a total concentration of 20 mg/mL (15 mg/mL for $Zn(L1)_2$) in o-DCB. The solutions were filtered through a 0.45µm PTFE filter prior to spin coating. All acceptors were blended with P3HT in 1:0.7 ratio except P3HT:$Zn(L1)_2$, which had a ratio of 1:0.5. The photoactive layers were pre-annealed at 120°C for 30 minutes followed by deposition of MoO_3 (10nm) and Ag (80nm) under a vacuum pressure of $3x10^{-5}$ Torr using the Angstrom Engineering Evovac Deposition System. Solar cell measurements were performed using an Oriel Sol2A solar simulator (AM 1.5, 100 mW/cm²) and Keithley 2400 source meter inside the glovebox. The devices have a total effective area of 0.20 cm². Incident Photon to Charge Carrier Efficiency (IPCE) was measured in air on fully constructed devices using a QEX10 Quantum Efficiency Measurement System.

For single-carrier device fabrication, ITO-coated glass substrates (R=15Ω/sq) were cleaned stepwise in soapy water, DI water, acetone and isopropanol under ultrasonication for 15 minutes followed to a UV-ozone treatment at 80°C for 15 minutes. For hole-only devices with an ITO/PEDOT:PSS/active layer/MoO_3/Ag structure, a layer of PEDOT:PSS was prepared by filtering through a 0.45µm PTFE filter followed by spin coating at 4000 rpm for 60 seconds and heated at 150°C for 10 minutes. The active layers were prepared in the same manner as for the photoactive layers. For electron-only devices with an ITO/ZnO/active layer/Ca/Al structure, cleaning of the ITO substrate, ZnO and active layer film formation was performed as previously described. Calcium (30nm) and Al (100nm) were thermally deposited. Dark current measurements for both architectures were performed using a Keithley 2400 source meter inside the glovebox. The devices have a total effective area of 0.20cm².

Atomic force microscopy was performed directly on the photoactive layer of photovoltaic devices using a Bruker Veeco Digital Instruments Dimension 3100 microscope and a Nanoscope IIIa controller in tapping mode. WSxM 5.0 Develop 8.0 was used to analyse the AFM images(29).

Results and discussion

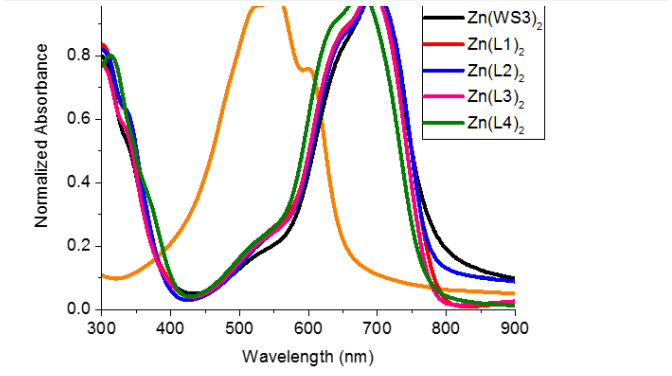

Fig. 4 Normalized UV-vis absorption spectra of neat films.

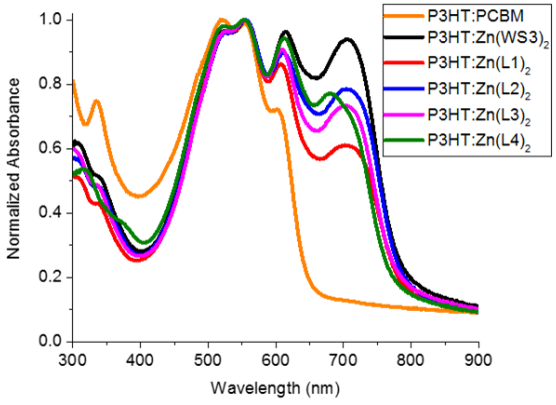

Fig. 5 Normalized UV-vis absorption spectra of acceptors blended films with P3HT.

Table 1 Summary of optical properties in neat and blended films.

	Neat Film		Blend Film		
	λ_{max} (nm)	λ_{onset} (nm)	λ_{max} (nm)	λ_{onset} (nm)	E_{opt} (eV)
$Zn(WS3)_2$	696	791	523, **555**, 614, 704	803	1.57
$Zn(L1)_2$	695	785	524, **555**, 607, 702	801	1.58
$Zn(L2)_2$	697	780	529, **553**, 609, 704	798	1.59
$Zn(L3)_2$	692	778	529, **554**, 609, 703	805	1.59
$Zn(L4)_2$	676	769	525, **553**, 612, 679	784	1.61

We have previously published the synthesis and purification of $Zn(L1\text{-}L4)_2$ and have shown ^1H NMR and elemental analysis in the supporting information of this publication as Figures S2-S6 and Tables S1-S4 (1). Figure 3 summarizes the estimated HOMO and LUMO energy levels of the zinc complexes from our previous publication (1). All complexes have deeper energy levels than P3HT and can therefore behave as acceptors when paired with P3HT. The optical properties of P3HT, $Zn(WS3)_2$ and the fluorinated acceptors in films are summarized in Figures 4-5 and Table 1. All zinc complexes have broad absorption from 500-800 nm and λ_{max} values of ~695nm. $Zn(L4)_2$ shows a slight blue shift compared to $Zn(WS3)_2$ of ~19 nm with a λ_{max} value of 676 nm. The λ_{onset} values of $Zn(WS3)_2$-$Zn(L4)_2$ are 791, 785, 780, 778, and 769 nm, respectively (1). The optical gap (E_{opt}) was estimated from the onset of neat films and averaged ~1.59eV for $Zn(WS3)_2$-$Zn(L4)_2$. These absorbance spectra are complementary to the absorption of P3HT, Fig. 4. To understand the absorption properties of our photoactive layer in solar cells, blend films were made under the same conditions as the solar cells. Films blended with P3HT and $Zn(WS3)_2$-$Zn(L4)_2$ showed λ_{max} values ~554 nm and λ_{onset} values of 803, 801, 798, 805, 784 nm, respectively. Compared to λ_{max} of the neat films, once blended with P3HT all of our acceptors show a redshift between 3-11 nm possibly due to different molecular pi-stacking in blends compared to neat films. While P3HT:PCBM absorbs from about 400-650 nm, P3HT:$Zn(WS3\text{-}L4)_2$ acceptor blends absorb light from 450 nm to 800 nm for a better overlap with the solar spectrum.

Photovoltaic properties were investigated using an inverted configuration: ITO/ZnO/P3HT:Acceptor/MoO_3/Ag. Device processing optimization involved screening for donor-to-acceptor blend ratios (1:0.25, 1:0.5, 1:0.7 and 1:1), solvent choice (chloroform and ortho-dichlorobenzne (o-DCB)), total concentration (15 mg/mL, 20 mg/mL and 30 mg/mL) and annealing conditions (as cast, 100°C for 10 mins, 100°C for 30 mins, 120°C for 10 mins, 120°C for 30 mins). The best results were obtained using a concentration of 20 mg/mL in o-DCB, a film thickness of ~100 nm and photoactive layer annealing conditions at 120°C for 30 mins. Figure 6 and Table 2 summarize the current density-voltage curves and photovoltaic performance parameters. Fluorinated acceptors blended with P3HT donor showed PCEs in the 2-4% range. The best performance of P3HT:$Zn(WS3)_2$ was obtained using a blend ratio of 1:0.7 and gave an open-circuit voltage (V_{OC}) of 0.81 V, a short-circuit current density (J_{SC}) of 5.7 mA/cm^2, a fill factor (FF) of 55% and PCEs of 2.5%. For devices containing P3HT:$Zn(L1)_2$ the best conditions were slightly different, with a blend ratio of 1:0.5, a concentration of 15 mg/mL, and a film thickness of ~90 nm. These conditions gave a V_{OC} of 0.68 V, a J_{SC} of 5.8 mA/cm^2, a FF of 52% and a PCE of 2.0%. For the other fluorinated acceptors $Zn(L2)_2$-$Zn(L4)_2$, the best results were obtained using the same conditions as for P3HT:$Zn(WS3)_2$. The best performance of P3HT:$Zn(L2)_2$ gave a V_{OC} of 0.72 V, a J_{SC} of 7.5 mA/cm^2, a FF of 56% and a PCE of 3.0%. The highest efficiency was obtained using P3HT:$Zn(L3)_2$ which gave a V_{OC} of 0.73 V, a J_{SC} of 8.5 mA/cm^2, a FF of 60% and a PCE of 3.7%. A blend of P3HT:$Zn(L4)_2$ gave a V_{OC} of 0.59 V, a J_{SC} of 9.3 mA/cm^2, a FF of 60% and a PCE of 3.3%. The lower V_{OC}'s obtained with $Zn(L1)_2$ and $Zn(L4)_2$ are consistent with their deeper LUMO energy levels than with $Zn(WS3)_2$ (Figure 2), and the V_{OC} of the $Zn(L4)_2$

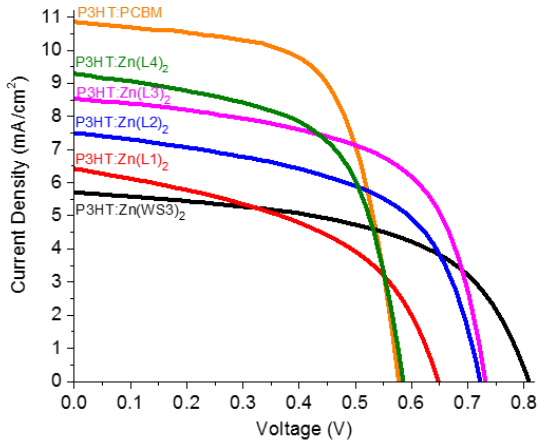

Fig. 6 Current density-voltage characteristics of solar cells.

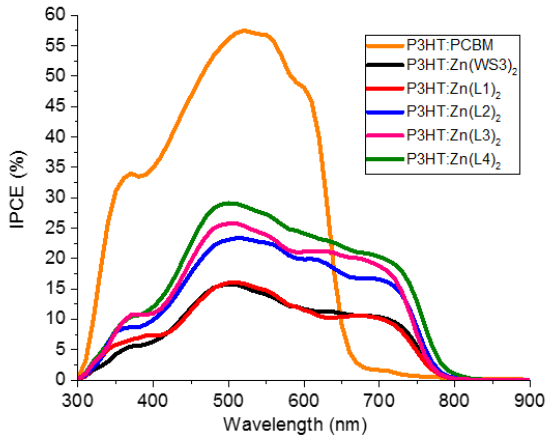

Fig. 7 Incident photon-to-current efficiency spectra of solar cell.

Table 2 Performance parameters of OPV and SCLC devices.

Acceptor	V_{OC} (V)	J_{SC} (mA cm^{-2})	FF	PCE (%)	Neat Film μ_h (cm^2 V^{-1} s^{-1})	Neat Film μ_e (cm^2 V^{-1} s^{-1})	Blend Film μ_h (cm^2 V^{-1} s^{-1})	Blend Film μ_e (cm^2 V^{-1} s^{-1})
PCBM	0.58 (0.58±0.02)	10.86 (10.59±0.68)	0.65 (0.63±0.02)	4.05 (3.90±0.10)	--	5.00×10^{-3}*	5.50×10^{-4}**	2.63×10^{-3}
$Zn(WS3)_2$	0.81 (0.77±0.03)	5.70 (5.40±0.68)	0.55 (0.52±0.06)	2.53 (2.14±0.14)	2.74×10^{-5}	1.40×10^{-5}	6.73×10^{-4}	5.82×10^{-5}
$Zn(L1)_2$	0.68 (0.66±0.01)	5.76 (5.50±0.49)	0.52 (0.48±0.04)	2.04 (1.74±0.23)	1.39×10^{-4}	2.47×10^{-4}	4.81×10^{-4}	1.02×10^{-5}
$Zn(L2)_2$	0.72 (0.71±0.02)	7.50 (7.08±0.66)	0.56 (0.56±0.03)	3.04 (2.80±0.16)	3.63×10^{-4}	3.77×10^{-4}	5.44×10^{-4}	6.87×10^{-4}
$Zn(L3)_2$	0.73 (0.71±0.01)	8.54 (7.36±0.73)	0.60 (0.56±0.02)	3.74 (3.07±0.34)	1.40×10^{-4}	1.31×10^{-3}	5.45×10^{-4}	2.63×10^{-3}
$Zn(L4)_2$	0.59 (0.57±0.02)	9.29 (7.81±0.93)	0.60 (0.60±0.02)	3.26 (2.67±0.36)	3.90×10^{-4}	1.07×10^{-3}	3.99×10^{-4}	6.50×10^{-4}

Averages were calculated from 10-15 devices. *Data is borrowed from Muth, et. al. (30). ** Data is borrowed from Mikie, et. al. (31)

device has a similar V_{OC} than the PCBM-based devices, consistent with its LUMO energy level being similar to that of PCBM. However, V_{OC} for the series ranged over 0.2V, larger than the 0.1eV range for the estimated LUMO energy levels. This discrepancy may be due to errors in the estimated LUMO levels, especially since they were obtained in solution instead of film. Efforts to obtain cyclic voltammograms of films of the Zn(II) complexes failed, as the films delaminated easily from the carbon electrodes. $Zn(L4)_2$ also showed the highest photocurrent of the non-fullerene acceptors tested, and is therefore the best candidate for pairing with high performance polymer donors that were optimized for PCBM and usually have lower lying energy levels than P3HT.

The maximum incident photon-to-current efficiencies (IPCEs) are shown in Figure 7. The spectral responses for the fullerene-free solar cells covered the visible spectra between 400 nm and 800 nm, comparable to the UV-vis spectra of the blend films and extending well beyond the absorption edge of P3HT at ~650 nm. This demonstrates that the acceptors participate in converting 600-800 nm wavelength light into current. The IPCE at 510 nm were 57%, 29%, 26%, 23%, 16% and 16% for PCBM and $Zn(L1)_2$-$Zn(L4)_2$ respectively, and are consisted with the photocurrent results. These IPCEs are low compared to the P3HT:PCBM control. The P3HT:PCBM film were thicker ~200 nm, and therefore absorbed more light than the P3HT: Zinc acceptor blends with thicknesses of ~100 nm. However, making the P3HT:Zinc acceptor blends thicker did not increase photocurrent, pointing to non-optical causes that limit performance in our fullerene-free devices.

To elucidate the reason for these low photocurrents, charge carrier mobility was estimated using the space-charge limited current (SCLC) model in neat and blend films. For hole mobility a device structure of ITO/PEDTO:PSS/Donor:Acceptor/MoO_3/Ag was used and for hole mobility a device structure of was used and for electron mobility a device structure of ITO/ZnO/Donor:Acceptor/Ca/Al was used (30). We attempted to estimate electron mobilities using other device structures (eg. ITO/Al/Donor:Acceptor/Al) but due to film formation issues on top of aluminium, mobilities were inconsistent. Our electron mobility structure mentioned above allowed for better film formation and higher mobilities. Table 2 and Figure 8 summarizes the mobility results. In neat films, all the zinc complexes showed a hole and electron mobility, suggesting these complexes are ambipolar. The fluorinated acceptors all showed higher hole and electron mobilities compared to unfluorinated $Zn(WS3)_2$, a positive outcome of fluorination. Hole mobility for $Zn(WS3)_2$ in a neat film was estimated to be 2.74×10^{-5} $cm^2V^{-1}s^{-1}$ while $Zn(L1)_2$ - $Zn(L4)_2$ showed a hole mobilities of 1.39×10^{-4}, 3.63×10^{-4}, 1.40×10^{-4} and 3.90×10^{-4} $cm^2V^{-1}s^{-1}$, respectively (Figure 8b). Electron mobilities for $Zn(WS3)_2$, $Zn(L1)_2$ and $Zn(L2)_2$ were similar to the hole mobilities with values of 1.40×10^{-5}, 2.47×10^{-4} and 3.77×10^{-4} $cm^2V^{-1}s^{-1}$ for neat films, respectively. Interestingly, $Zn(L3)_2$ and $Zn(L4)_2$ showed much higher electron mobilities, as high as 1.31×10^{-3} and 1.07×10^{-3} $cm^2V^{-1}s^{-1}$ for $Zn(L3)_2$ and $Zn(L4)_2$, respectively (Figure 8e). Both $Zn(L3)_2$ and $Zn(L4)_2$ were fluorinated on the phenylethynyl groups, suggesting that these groups play a significant role in increased charge mobility. Since these complexes are non-planar, charge transport can only occur if certain conjugated parts of the molecule can π-stack with other parts of an adjacent molecule. The published crystal structure of $Zn(L2)_2$ shows that these intermolecular π-interactions can occur with the phenyls protruding from the molecular core: at the distal phenyls and the pyrrolic phenylethynyls (1). Since the complex is highly conjugated, only 2 out of the 8 protruding phenyls need to interact with their neighbours in order to form a conductive path. These acceptors can therefore have random orientations while maintaining good charge transport properties. Indeed, Grazing incident wide-angle X-ray scattering experiments for P3HT:$Zn(WS3)_2$ showed at $Zn(WS3)_2$ is completely amorphous (28). Fluorination has been suggested as a way to enhance crystal packing, electronic coupling, and mobility for naphthalenes and perylenes (32, 33). We hypothesize that fluorination of the phenylethynyl groups may be enhancing electronic coupling between adjacent complexes

and points to the phenylethynyl groups as key for charge transport in these materials.

In P3HT:acceptor blend films, the hole mobilities were similar, ranging from 6.7 x 10^{-4} $cm^2V^{-1}s^{-1}$ to 4.0 x 10^{-4} $cm^2V^{-1}s^{-1}$ (Figure 8c), similar to hole mobilities measured in P3HT:PCBM control devices and consistent with hole transport occurring in the P3HT (34). The presence of Zn(II)

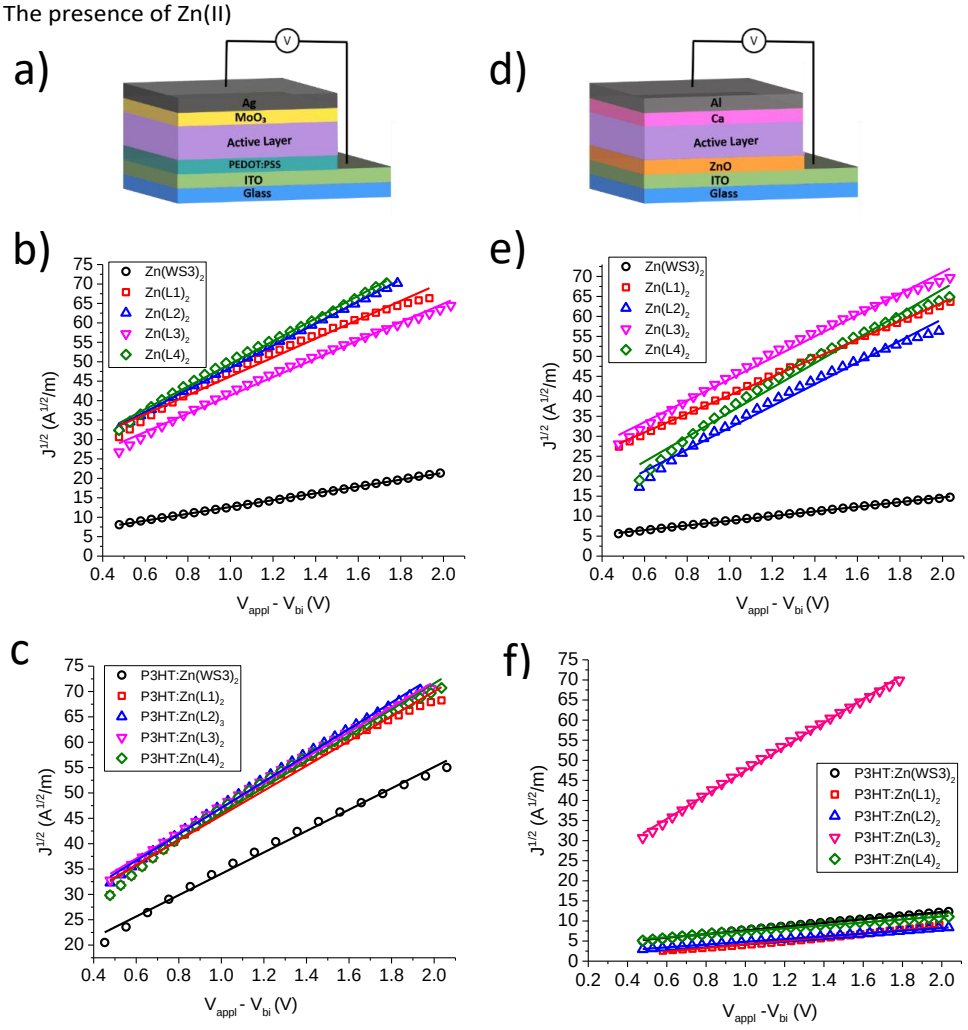

Fig. 8 Hole mobility; a) hole-only device structure b) $J^{1/2}$ characteristics of hole-only mobility in neat films c) $J^{1/2}$ characteristics of hole-only mobility in P3HT:Acceptor blend films. Electron mobility; d) electron-only device structure e) $J^{1/2}$ characteristics of electron-only mobility in neat films f) $J^{1/2}$ characteristics of electron-only mobility in P3HT:Acceptor blend films.

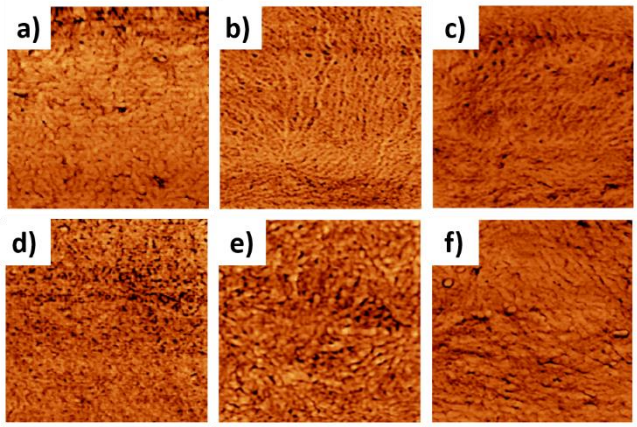

Fig. 9 1x1µm AFM phase images. (a) P3HT:PCBM. (b) P3HT:Zn(WS3)$_2$. (c) P3HT:Zn(L1)$_2$. (d) P3HT:Zn(L2)$_2$. (e) P3HT:Zn(L3)$_2$. (f) P3HT:Zn(L4)$_2$.

complexes therefore did not negatively affect P3HT self-assembly. Electron mobilities, on the other hand, varied greatly from 1.0 x 10^{-5} $cm^2V^{-1}s^{-1}$ for Zn(L1)$_2$ to 6.9 x 10^{-4} $cm^2V^{-1}s^{-1}$ for Zn(L2)$_2$ and 6.5 x 10^{-4} $cm^2V^{-1}s^{-1}$ for Zn(L4)$_2$, to a high 2.6 x 10^{-3} $cm^2V^{-1}s^{-1}$ for Zn(L3)$_2$ (Figure 8f). The later is similar to the electron mobility found in P3HT:PCBM control devices, and is therefore high enough to yield high efficiency organic solar cells. In fact, three of our acceptors with PCEs in the 3-4% range showed charge carrier mobilities that are high enough to result for high performance devices. The ability for these acceptors to transport charges is therefore not limiting their photocurrent.

Photocurrent is known to be strongly affected by the morphology of blend film (35, 36). With this in mind, we imaged the film surface of the photoactive layer in fully constructed OPVs by atomic force microscopy (AFM) in the tapping mode. While AFM is limited to imaging the surface, it provides useful information such as domain size, interconnectivity and surface roughness, all related to charge generation and transport of OPVs. Furthermore, AFM may provide a rough scale determination of exciton diffusion length of the donor:acceptor interphase. Figure 9 shows the 1x1µm phase images for the OPV photoactive layers. The corresponding 1 x 1µm heights images and 10 x 10um images can be found in the supporting information section. While the images are slightly different for each acceptor, they all show favorable nanoscale phase separation between the P3HT and acceptor, and all show P3HT nanofibril formation for efficient hole transport (37-39). There is no indication of large scale phase separation or self-aggregation. Surface roughness of the 1 x 1µm images are 16.6, 12.0, 13.8, 13.7, 8.63 and 9.79 nm for PCBM, Zn(WS3)$_2$ and Zn(L1)$_2$-Zn(L4)$_2$, respectively. While Zn(WS3)$_2$ and Zn(L1)$_2$-Zn(L2)$_2$ have similar RMS values to our P3HT:PCBM control and reported values, Zn(L3)$_2$-Zn(L4)$_2$ show a smoother surface (40). To a first approximation, film morphology does not appear to limit photocurrents. Although a more detailed study is required to fully assess the role of morphology on device performance in these systems, we suspect that features that are very difficult to image, such as mixed phase morphology and donor:acceptor interfaces, may be most relevant.

Other factors that strongly affect photocurrent are exciton splitting, charge separation and charge collection efficiencies (41, 42). We have previously shown that exciton splitting is efficient with these types of acceptors (27). One factor that may strongly limit charge collection efficiency is bimolecular recombination between a free hole and a free electron. To better understand charge recombination, light-intensity dependence on photocurrent was investigated. J_{sc} has a power-law dependence on P_{light} ($J_{sc} \propto P_{light}^{\alpha}$) where α is the power-law component. As α approaches unity, bimolecular recombination is negligible and insignificant (43). Figure 10 shows fitted α values for blended films. While P3HT:PCBM shows the highest α value at 0.99, all of the Zn(II) acceptors show an α value <1. In fact, the α value correlates well with the photocurrents observed (Figure 11). The fluorinated acceptors showed less bimolecular recombination than Zn(WS3)$_2$, consistent with their higher photocurrents observed in devices. While Zn(L1)$_2$ shows a very similar α-value as Zn(WS3)$_2$, acceptors Zn(L2)$_2$ - Zn(L4)$_2$ show larger α-values (0.74, 0.81 and 0.86, respectively)

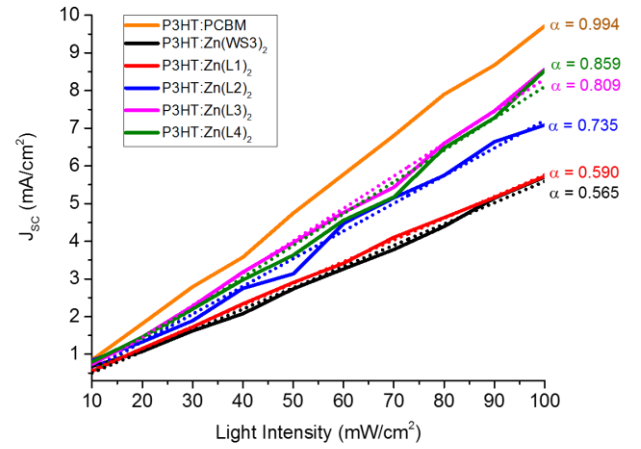

Fig. 10 Bimolecular recombination estimates.

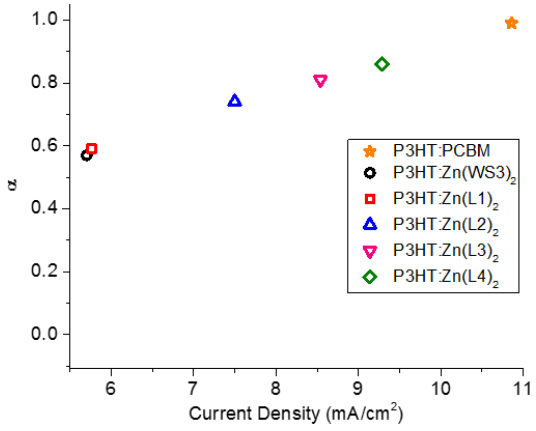

Fig. 11 Power-law component (α) versus J_{SC}.

suggesting the addition of fluorine in the distal and phenylethynyl positions play a role in suppressing bimolecular recombination in our acceptors. This suppression of bimolecular recombination could be due to morphology improvements, less hard-to-detect impurities or traps in the complexes, enhanced electron transport out of mixed phases, or a combination of these possibilities.

Conclusions

We studied the effect of a single fluorine atom in three different positions on the parent compound, $Zn(WS3)_2$ and the degree of fluorination in the pyrrolic position using CF_3. While fluorination has little effect on the absorbance spectra and on energy levels, it strongly affected charge transport, bimolecular recombination and device performance. Generally, fluorination increased the PCE in OPVs from 2.5% of $Zn(WS3)_2$ to 3.7% in $Zn(L3)_2$. The highest photocurrent was observed in $Zn(L4)_2$ which contains a CF_3 group in the pyrrolic position. Combined with its lower LUMO energy level than $Zn(WS3)_2$, these results suggest that $Zn(L4)_2$ has potential to be paired with donors that have lower-lying energy levels than P3HT. AFM reveals a favorable nanoscale morphology and lack of large aggregation in all of our blends, similar to P3HT:PCBM. Bimolecular recombination studies reveal that recombination limits PCE in these fullerene-free devices, and that fluorine substitutions suppress bimolecular recombination. Finally, our mobility measurements reveal that all of our fluorinated acceptors have higher neat film mobilities than $Zn(WS3)_2$. $Zn(L3)_2$ and $Zn(L4)_2$ revealed very high electron mobilities similar to that of PCBM. These results point to the importance of the pyrrolic phenylethylnyls in optimizing charge transport and device performance for this type of acceptor.

Conflicts of interest

There are no conflicts to declare.

Acknowledgements

The authors gratefully acknowledge the National Science Foundation (CHEM 1148652) for supporting this project. We also thank the Materials for Optoelectronics Research and Education (MORE) Center at CWRU for providing instrumentation and equipment and Dr. Ina Martin for providing support and guidance on device fabrication and characterization. Finally, we thank Richard Tomazin and the Swagelok Center for Surface Analysis of Materials (SCSAM) at CWRU for providing instrumentation and guidance with atomic force microscopy.

Notes and references

1. Etheridge FS, Fernando RJ, Pejic S, Zeller M, Sauve G. Synthesis and characterization of fluorinated azadipyrromethene complexes as acceptors for organic photovoltaics. *Beilstein J Org Chem*. 2016;12:1925-38.
2. Do K, Saleem Q, Ravva MK, Cruciani F, Kan Z, Wolf J, et al. Impact of Fluorine Substituents on pi-Conjugated Polymer Main-Chain Conformations, Packing, and Electronic Couplings. *Adv Mater*. 2016;28(37):8197-205.
3. Jung JW, Jo JW, Chueh CC, Liu F, Jo WH, Russell TP, et al. Fluoro-Substituted n-Type Conjugated Polymers for Additive-Free All-Polymer Bulk Heterojunction Solar Cells with High Power Conversion Efficiency of 6.71. *Adv Mater*. 2015;27(21):3310-7.
4. Jung JW, Jo WH. Low-Bandgap Small Molecules as Non-Fullerene Electron Acceptors Composed of Benzothiadiazole and Diketopyrrolopyrrole for All Organic Solar Cells. *Chem Mater*. 2015;27(17):6038-43.
5. Leclerc N, Chávez P, Ibraikulov O, Heiser T, Lévêque P. Impact of Backbone Fluorination on π-Conjugated Polymers in Organic Photovoltaic Devices: A Review. *Polym*. 2016;8(1):11.
6. Wang Z, Li Z, Liu J, Mei J, Li K, Li Y, et al. Solution-Processable Small Molecules for High-Performance Organic Solar Cells with Rigidly Fluorinated 2,2'-Bithiophene Central Cores. *ACS Appl Mater Interfaces*. 2016;8(18):11639-48.
7. Babudri F, Farinola GM, Naso F, Ragni R. Fluorinated organic materials for electronic and optoelectronic applications: the role of the fluorine atom. *Chem Commun*. 2007(10):1003-22.
8. Weller T, Breunig M, Mueller CJ, Gann E, McNeill CR, Thelakkat M. Fluorination in thieno[3,4-c]pyrrole-4,6-dione copolymers leading to electron transport, high crystallinity and end-on alignment. *J Mater Chem C*. 2017;5(30):7527-34.
9. Lei T, Xia X, Wang JY, Liu CJ, Pei J. "Conformation locked" strong electron-deficient poly(p-phenylene vinylene) derivatives for ambient-stable n-type field-effect transistors: synthesis, properties, and effects of fluorine substitution position. *J Am Chem Soc*. 2014;136(5):2135-41.
10. Newman CR, Frisbie CD, de Silva Filho DA, Bredas J-L, Ewbank PC, Mann KR. Introduction to Organic Thin Film Transistors and Design of n-Channel Organic Semiconductors *Chem Mater*. 2004;16:4436-51.
11. Xu T, Yu L. How to design low bandgap polymers for highly efficient organic solar cells. *Mater Today*. 2014;17(1):11-5.
12. Fei Z, Boufflet P, Wood S, Wade J, Moriarty J, Gann E, et al. Influence of Backbone Fluorination in Regioregular Poly(3-alkyl-4-fluoro)thiophenes. *J Am Chem Soc*. 2015;137(21):6866-79.
13. Mei J, Diao Y, Appleton AL, Fang L, Bao Z. Integrated materials design of organic semiconductors for field-effect transistors. J Am Chem Soc. 2013;135(18):6724-46.
14. Zhao W, Li S, Yao H, Zhang S, Zhang Y, Yang B, et al. Molecular Optimization Enables over 13% Efficiency in Organic Solar Cells. J Am Chem Soc. 2017;139(21):7148-51.
15. Yang P, Yuan M, Zeigler DF, Watkins SE, Lee JA, Luscombe CK. Influence of fluorine substituents on the film dielectric constant and open-circuit voltage in organic photovoltaics. *J Mater Chem C*. 2014;2(17):3278-84.
16. Stuart AC, Tumbleston JR, Zhou H, Li W, Liu S, Ade H, et al. Fluorine substituents reduce charge recombination and drive structure and morphology development in polymer solar cells. *J Am Chem Soc*. 2013;135(5):1806-15.
17. Carsten B, Szarko JM, Son HJ, Wang W, Lu L, He F, et al. Examining the effect of the dipole moment on charge separation in donor-acceptor polymers for organic photovoltaic applications. *J Am Chem Soc*. 2011;133(50):20468-75.
18. Liu Y, Zhao J, Li Z, Mu C, Ma W, Hu H, et al. Aggregation and morphology control enables multiple cases of high-efficiency polymer solar cells. *Nat Commun*. 2014;5:5293.

19. He YaL, Yongfang. Fullerene derivative acceptors for high performance polymer solar cells *Phys Chem Chem Phys* 2010;13:1970-83.
20. Peet J, Senatore ML, Heeger AJ, Bazan GC. The Role of Processing in the Fabrication and Optimization of Plastic Solar Cells. *Adv Mater*. 2009;21(14-15):1521-7.
21. Hou J, Inganas O, Friend RH, Gao F. Organic solar cells based on non-fullerene acceptors. Nat Mater. 2018;17(2):119-28.
22. Zhao W, Qian D, Zhang S, Li S, Inganas O, Gao F, et al. Fullerene-Free Polymer Solar Cells with over 11% Efficiency and Excellent Thermal Stability. Adv Mater. 2016;28(23):4734-9.
23. Yao Z, Liao X, Gao K, Lin F, Xu X, Shi X, et al. Dithienopicenocarbazole Based Acceptors for Efficient Organic Solar Cells with Optoelectronic Response Over 1000 nm and an Extremely Low Energy Loss. J Am Chem Soc. 2018.
24. Xiao Z, Jia X, Ding L. Ternary organic solar cells offer 14% power conversion efficiency. Science Bulletin. 2017;62(23):1562-4.
25. Xiao Z, Jia X, Li D, Wang S, Geng X, Liu F, et al. 26 mA cm −2 J sc from organic solar cells with a low-bandgap nonfullerene acceptor. Science Bulletin. 2017;62(22):1494-6.
26. Xiao Z, Liu F, Geng X, Zhang J, Wang S, Xie Y, et al. A carbon-oxygen-bridged ladder-type building block for efficient donor and acceptor materials used in organic solar cells. Science Bulletin. 2017;62(19):1331-6.
27. Senevirathna W, Liao J-y, Mao Z, Gu J, Porter M, Wang C, et al. Synthesis, characterization and photovoltaic properties of azadipyrromethene-based acceptors: effect of pyrrolic substituents. *J Mater Chem A*. 2015;3(8):4203-14.
28. Mao Z, Senevirathna W, Liao JY, Gu J, Kesava SV, Guo C, et al. Azadipyrromethene-based Zn(II) complexes as nonplanar conjugated electron acceptors for organic photovoltaics. *Adv Mater*. 2014;26(36):6290-4.
29. Horcas I, et. a. Rev Sci Instrum 2007;78(013705).
30. Muth MA, Mitchell W, Tierney S, Lada TA, Xue X, Richter H, et al. Influence of charge carrier mobility and morphology on solar cell parameters in devices of mono- and bis-fullerene adducts. *Nanotechnology*. 2013;24(48):484001.
31. Mikie T, Saeki A, Ikuma N, Kokubo K, Seki S. Hetero Bis-Addition of Spiro-Acetalized or Cyclohexanone Ring to 58pi Fullerene Impacts Solubility and Mobility Balance in Polymer Solar Cells. *ACS Appl Mater Interfaces*. 2015;7(23):12894-902.
32. Dunitz JDT, R. Organic Fluorine Hardly Ever Accepts Hydrogen Bonds. *Chem Eur J*. 1997;3(1):89-98.
33. Reichenbacher K, Suss HI, Hulliger J. Fluorine in crystal engineering--"the little atom that could". *Chem Soc Rev*. 2005;34(1):22-30.
34. Ahmed MFH, I.A. . Determination of Electron and Hole Mobility in Poly(3-hexylthiophene) Usine Space-Charge-Limited-Current Measurements. *Int J Electroactive Materials* 2013;1:60-3.
35. Ostrowski DP, Vanden Bout DA. Correlation of morphology with photocurrent generation in a polymer blend photovoltaic device. *Small*. 2014;10(9):1821-9.
36. Utzat H, Dimitrov SD, Wheeler S, Collado-Fregoso E, Tuladhar PS, Schroeder BC, et al. Charge Separation in Intermixed Polymer:PC70BM Photovoltaic Blends: Correlating Structural and Photophysical Length Scales as a Function of Blend Composition. *J Phys Chem C*. 2017;121(18):9790-801.
37. Zhang X, Yuan N, Ding S, Wang D, Li L, Hu W, et al. Growth and carrier-transport performance of a poly(3-hexylthiophene)/1,2,3,4-bis(p-methylbenzylidene) sorbitol hybrid shish-kebab nanostructure. *J Mater Chem C*. 2017;5(16):3983-92.
38. Lee Y, Oh JY, Son SY, Park T, Jeong U. Effects of Regioregularity and Molecular Weight on the Growth of Polythiophene Nanofibrils and Mixes of Short and Long Nanofibrils To Enhance the Hole Transport. *ACS Appl Mater Interfaces*. 2015;7(50):27694-702.
39. Zhao Y, Shao S, Xie Z, Geng Y, Wang L. Effect of Poly(3-hexylthiophene) Nanofibirls on Charge Separation and Transport in Polymer Bulk Heterojunction Photovoltaic Cells. *J Phys Chem C*. 2009;113:17235-9.
40. Li G, Shrotriya V, Huang J, Yao Y, Moriarty T, Emery K, et al. High-efficiency solution processable polymer photovoltaic cells by self-organization of polymer blends. *Nat Mater*. 2005;4(11):864-8.
41. Philippa B, Stolterfoht M, Burn PL, Juska G, Meredith P, White RD, et al. The impact of hot charge carrier mobility on photocurrent losses in polymer-based solar cells. *Sci Rep*. 2014;4:5695.
42. Nelson J. Polymer:fullerene bulk heterojunction solar cells. *Mater Today*. 2011;14(10):462-70.
43. Gao L, Zhang ZG, Xue L, Min J, Zhang J, Wei Z, et al. All-Polymer Solar Cells Based on Absorption-Complementary Polymer Donor and Acceptor with High Power Conversion Efficiency of 8.27%. *Adv Mater*. 2016;28(9):1884-90.

Strategic fluorination of non-planar electron acceptors reduces bimolecular recombination in OPVs and significantly enhances electron mobility, ~10^{-3} cm^2/Vs in diodes.